Time-resolved study of the symmetric S_N2-reaction $I^- + CH_3I$

Roland Wester,[a] Arthur E. Bragg, Alison V. Davis, and Daniel M. Neumark[b]
Department of Chemistry, University of California—Berkeley, Berkeley, California 94720, and Chemical Sciences Division, Lawrence Berkeley National Laboratory, Berkeley, California 94720

(Received 2 May 2003; accepted 22 August 2003)

Time-resolved photoelectron spectroscopy of negative ions has been applied to study the title reaction as a model system for gas phase S_N2 reactions. Starting from the precursor cluster $I_2^- \cdot CH_3I$, the interaction of the reactants I^- and CH_3I is initiated by a pump pulse and the subsequent dynamics are observed with a delayed probe pulse used to detach the excess electron and measure their photoelectron spectra. Using two different pump photon energies, which lead to different amounts of internal energy available to the reaction complex, a number of dynamical features have been observed. For small internal excitation, the reactants only form stable, albeit vibrationally excited, $I^- \cdot CH_3I$ complexes. However, with increased internal excitation, complexes are formed that exhibit biexponential decay back to I^- and CH_3I reactants with time scales of 0.8 and 10 ps. Similar dynamics are expected for entrance channel complex formed in the first step of a gas phase S_N2 reaction. © *2003 American Institute of Physics.* [DOI: 10.1063/1.1618220]

I. INTRODUCTION

Bimolecular nucleophilic substitution (S_N2) reactions, $X^- + RY \rightarrow RX + Y^-$, have been extensively investigated owing to the importance of this model reaction mechanism in physical organic chemistry.[1–4] Interest in gas phase studies of the kinetics and dynamics of S_N2-reactions has centered on trying to disentangle their intrinsic properties from effects induced in solution. Much of this work was inspired by Brauman's pioneering studies 25 years ago,[5] in which the kinetics for a series of gas phase S_N2-reactions were interpreted in terms of a double minimum potential, as opposed to the single reaction barrier used to explain S_N2-reactions in solution. Many experiments have focused on the measurement of reaction rate constants and cross sections,[6–13] but in recent years the energy partitioning among final states has been investigated using translational energy spectroscopy,[14] while photofragment and photoelectron spectroscopy have been employed to study the entrance and exit channel complexes of S_N2-reactions.[15–17] Theoretical studies have focused on both *ab initio* calculations of potential energy surfaces[18–21] and classical and quantum dynamics calculations on these surfaces[1,22,23] (see Ref. 4 for an exhaustive list of references).

Although kinetics results on gas phase S_N2 reactions were originally interpreted within the framework of statistical reaction rate theories, there is now a fair body of evidence showing significant deviations from the predictions of statistical models.[1] This nonstatistical behavior manifests itself in different rate coefficients depending on whether reactants are translationally or vibrationally excited[24] and it also leads to stronger vibrational excitation of the products than expected statistically.[14] Many aspects of these nonstatistical dynamics have been elucidated using both classical trajectory calculations[1,22,25] and reduced-dimensionality quantum scattering calculations.[23,26]

These experimental and theoretical results motivate the work presented here, in which we attempt the first time-resolved investigation of a bimolecular S_N2-reaction in the gas phase. Our work focuses on the symmetric S_N2 reaction,

$$I^- + CH_3I \rightarrow CH_3I + I^- \quad (1)$$

using anion femtosecond photoelectron spectroscopy (FPES),[27] a technique that has so far been used successfully to follow dynamics in vibrationally or electronically excited molecular anions[28] and anion clusters.[29,30] While we cannot distinguish reactants from products in this symmetric reaction, we can investigate the dynamics of the $I^- \cdot CH_3I$ intermediate in real time, with the goal of following the reactants along the reaction coordinate and directly measuring the time duration of individual reaction steps.

Previous experiments aimed at extracting information on the potential energy surface for reaction (1), have focused on the ion-dipole complex $I^- \cdot CH_3I$. This species was investigated in a series of experiments by Johnson and co-workers.[15,16,31–33] Using photoelectron and photofragment spectroscopy, Cyr *et al.*[15,32] determined the anion cluster binding energy to be 0.38 eV based on the solvent shift between the PE spectra of I^- and $I^- \cdot CH_3I$, and observed vibrational structure in the PE spectrum resulting from distortion of the CH_3I in the anion complex. Further studies focused on the dynamics of the charge transfer excited states.[16,31] Arnold *et al.*[33] investigated the van der Waals modes of the neutral $I \cdot CH_3I$ ground state using anion ZEKE spectroscopy of $I^- \cdot CH_3I$.

Electronic structure calculations yielding the geometry, vibrational frequencies, and binding energy of $I^- \cdot CH_3I$ were carried out by Hu *et al.*[34] They obtained a slightly lower well depth of 0.34 eV, and attributed the higher experimental value to a repulsive interaction between neutral I and CH_3I

[a]Present address: Physikalisches Institut, Universität Freiburg, Hermann-Herder-Str. 3, 79104 Freiburg, Germany.
[b]Author to whom correspondence should be addressed. Electronic mail: dan@radon.cchem.berkeley.edu

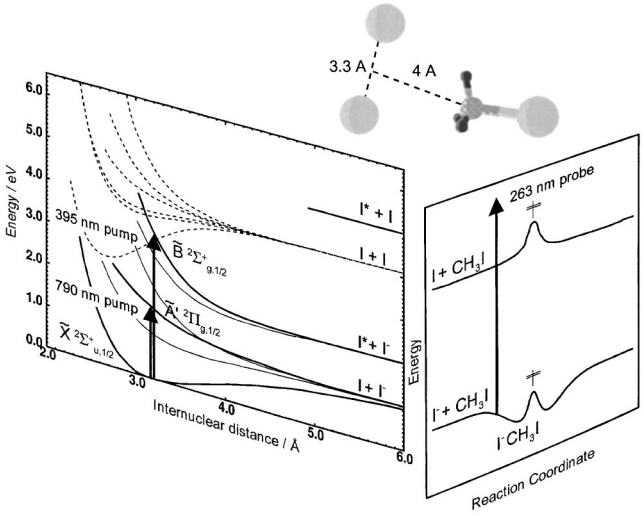

FIG. 1. Schematic potential energy diagrams of I_2^- and $I^- \cdot CH_3I$. The depicted structure of the I_2^- CH_3I precursor complex represents the result of our *ab initio* calculation.

which leads to a solvent shift larger than the anion binding energy. They also calculated the distance of the I^- from the carbon in CH_3I to be 3.4 Å. The reaction coordinate for reaction (1) was investigated in electronic structure calculations by Glukhovtsev *et al.*[19] They found the central barrier at the transition state to be 70 meV above the energy of the separated reactants.

No measurements of rate constants or cross sections for reaction (1) have been carried out to date, although experimental results are available for the related $Cl^- + CH_3Cl$ reaction.[6,9,11] These measurements have shown that very little reaction occurs until the collision energy is significantly higher than the central barrier height. At low energies, the bimolecular dynamics are expected to be dominated by complex formation and decay back to reactants, a process studied in detail in classical trajectory calculations by Hase and co-workers.[35–37]

Our time-resolved experiments probe the analogous dynamics in reaction (1). We use an experimental approach related to that developed by several groups[38–41] for neutral bimolecular reactions, in which the reactants are prepared in a precursor cluster such that a pump laser pulse initiates the reaction. In our experiments, we start with $I_2^- \cdot CH_3I$ clusters as precursors for the study of reaction (1).

The principle of the experiment is illustrated in Fig. 1. A femtosecond pump pulse is used to dissociate the I_2^- chromophore at either of two strong absorption bands at 790 and 395 nm, corresponding to excitation to the repulsive $A'\,^2\Pi_{g,1/2}$ and $B\,^2\Sigma_g^+$ states, respectively.[42] Subsequent to photodissociation, the neutral iodine will have left the cluster. The S_N2 reactants I^- and CH_3I, which are more strongly coupled due to their charge–dipole interaction, remain in close proximity to one another and can undergo reaction (1). The time-dependent dynamics are probed using a second femtosecond pulse that detaches the excess electron. By measuring PE spectra as a function of pump–probe delay, one can map the intermediate states and follow their temporal evolution. The use of two different pump wavelengths reveals how these dynamics depend on the relative kinetic energy between the I^- and CH_3I.

II. EXPERIMENT

The experiment is carried out using our femtosecond photoelectron spectroscopy setup described in detail in previous publications.[28,43] In short, a beam of mass-selected $I_2^- \cdot CH_3I$ clusters is crossed with femtosecond pump and probe pulses in the focus of a magnetic bottle electron spectrometer, and photoelectron kinetic energy spectra are measured as a function of pump–probe delay.

The $I_2^- \cdot CH_3I$ clusters are produced by passing 0.05% CH_3I in argon over solid iodine and supersonically expanding the gas mixture into vacuum through a pulsed nozzle that is operated at 500 Hz. Near the nozzle the neutral beam is crossed with a 1.2 keV electron beam. The cluster anions are formed in this supersonic expansion by attachment of slow secondary electrons to I_2 and subsequent clustering to a methyl iodide molecule. The anion pulses are accelerated to 1.6 keV kinetic energy using a Wiley–McLaren time-of-flight mass spectrometer that puts the time focus of the desired ion mass at the interaction point with the femtosecond laser pulses. Electrostatic deflectors and lenses steer the ion beam into optimal spatial overlap with the laser pulses.

The femtosecond pump and probe pulses that intercept the $I_2^- \cdot CH_3I$ clusters are produced with an amplified Ti:sapphire laser (CPA 1000 from Clark MXR) that delivers 80 fs pulses at a wavelength of 790 nm and with an energy of 1 mJ per pulse. The 500 Hz repetition rate of the laser matches the repetition rate of the pulsed anion cluster source. The output of the CPA 1000 is split into two paths, with 88% used to pump a frequency doubling and tripling stage, producing 395 nm pump pulses with 60 μJ per pulse and 263 nm probe pulses with 25 μJ per pulse. The remaining pulse energy at 790 nm (120 μJ per pulse) is used as an alternative pump pulse in this experiment. The pump and probe pulses are overlapped spatially and are then crossed with the cluster ion beam. Temporal synchronization of the laser pulses and the ion beam is achieved by using the femtosecond laser as the master trigger for the entire experiment. The pump–probe delay time is controlled by an optical delay stage (Newport). The cross correlation of the two pulses (about 200 fs FWHM) and thus the delay time zero is determined at the interaction point with the ions by measuring the above threshold detachment (ATD) intensity for I^- ions.

Photoelectrons detached by the probe pulse are analyzed with a magnetic bottle time-of-flight spectrometer. The time-of-flight spectra are recorded with a multichannel scaler (SR430 from Stanford Research Systems) integrating over typically 50 000 laser shots at each pump–probe delay time. The probe laser and the 395 pump laser produce significant background signal via one-photon detachment of $I_2^- \cdot CH_3I$. The background spectrum from the probe laser is automatically subtracted from the pump–probe spectra in the multichannel scaler by means of a rotating-wheel chopper that blocks the pump laser pulse for every other probe laser pulse. All pump–probe spectra are scaled to the intensity of these single-photon probe-only spectra, which corrects for drifts in

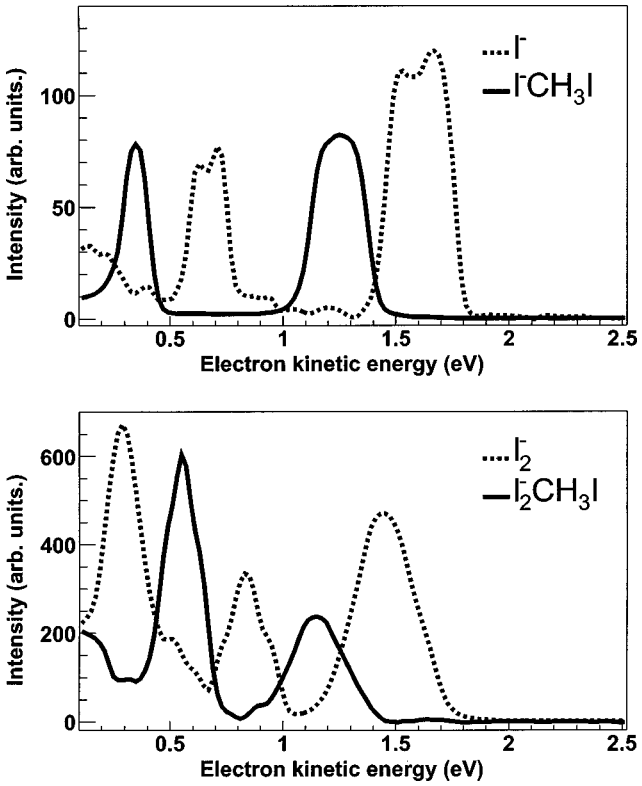

FIG. 2. Upper panel: Single photon photoelectron spectra at 263 nm for $I^- \cdot CH_3I$ (solid line) and I^- (dashed line); Lower panel: Single photon PE spectra for $I_2^-CH_3I$ (solid line) and I_2^- (dashed line). Note the 300 meV solvent shift of I_2^- when bound to CH_3I.

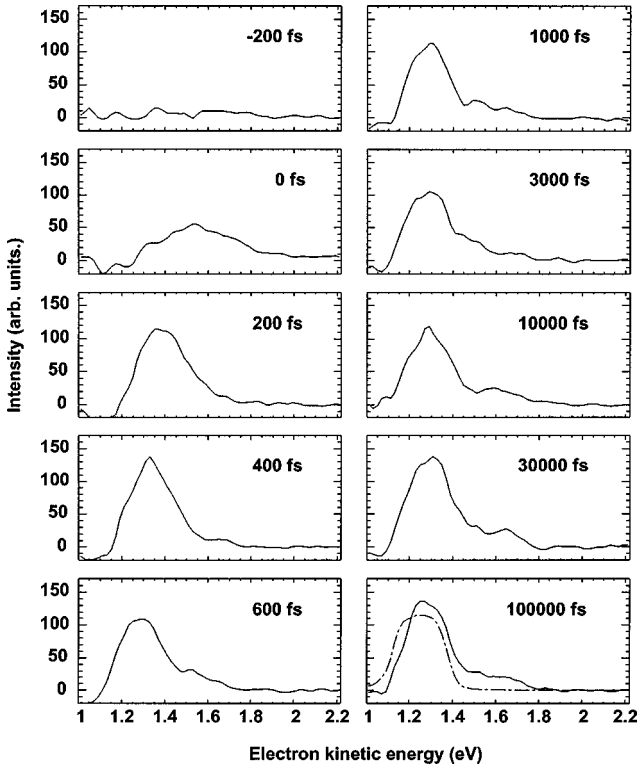

FIG. 3. Sequence of photoelectron spectra for pump–probe delay times between −200 fs and 100 ps using 790 nm pump pulses. From 500 fs onward the spectra remain unchanged. The PE spectrum of cold $I^- \cdot CH_3I$ is shown as the dashed–dotted line in the last panel.

the intensity of the cluster ion beam. The background spectrum from the 395 nm pump beam is recorded with each data set and is subtracted in the subsequent analysis. Finally, each time-of-flight spectrum is converted into an electron kinetic energy (eKE) spectrum, calibrated against a photoelectron spectrum of I^- and smoothed by folding it with a Gaussian of 50 meV FWHM.

The FWHM of the two discrete photodetachment lines in the I^- spectrum yields the overall energy resolution of the spectrometer of 190 meV at eKE = 0.7 eV and 270 meV at eKE = 1.6 eV. This relatively low resolution results from Doppler broadening of the photoelectrons detached from the fast ion beam.[44]

III. RESULTS

The upper panel of Fig. 2 shows the probe-only PE spectra of $I^- \cdot CH_3I$ (solid line) and of bare I^- (dashed line), while the lower panel shows the probe-only spectra of $I_2^- \cdot CH_3I$ (solid line) and of bare I_2^- (dashed line). All spectra are measured under the same experimental conditions as the pump–probe spectra described below. The I_2^- spectrum shows the three characteristic *X*, *A*, and *B* bands which, in contrast to our earlier PE spectra,[45] do not show any vibrational structure owing to the lower energy resolution in this experiment. The spectrum of $I_2^- \cdot CH_3I$ resembles that of I_2^-, but is shifted to lower eKE by a solvent shift of about 0.30 eV. This shift represents, to first order, the binding energy of I_2^- to CH_3I.

Figure 3 shows a sequence of measured photoelectron spectra of $I_2^- \cdot CH_3I$ for increasing pump–probe delay times using $\lambda_{pump} = 790$ nm and $\lambda_{probe} = 263$ nm (solid lines). The left column shows spectra with short delay times of −200 to 600 fs and the right column shows data for longer delay times, from 1 ps up to 100 ps. Data are shown only for eKE > 1.0 eV; the signal-to-noise ratio at lower eKE is considerably poorer and the data in that region are less useful.

When the probe pulse precedes the pump pulse (at −200 fs), no signal is visible, since all single-photon contributions have been subtracted. Within 200 fs after the pump pulse, a strong spectral feature appears around eKE = 1.4 eV with a width of ~200 meV (FWHM). It shifts by 100 meV to lower eKE (i.e., to 1.3 eV) within a few hundred femtoseconds leaving a small tail to higher energies. This shift is finished by 0.5 ps, after which no further spectral changes are observed, indicating no additional dynamics are occurring.

At $\lambda_{pump} = 395$ nm, the time sequence of photoelectron spectra (shown in Fig. 4) shows more involved dynamics. The initial fast increase of a spectral feature at 1.4 eV also seen for $\lambda_{pump} = 790$ nm is clearly visible, and overall, the spectra up to 400 fs delay time look remarkably similar for both pump wavelengths. But after 600 fs, the PE spectra start to broaden toward higher eKE, while the peak amplitude in the spectra decreases. By 1000 fs, the PE spectrum spans an eKE interval from 1.25 to 1.7 eV. For pump–probe delay times longer than 1 ps the width of the photoelectron spectrum remains essentially constant but its structure changes considerably. Between 1 and 3 ps, we observe a single, broad

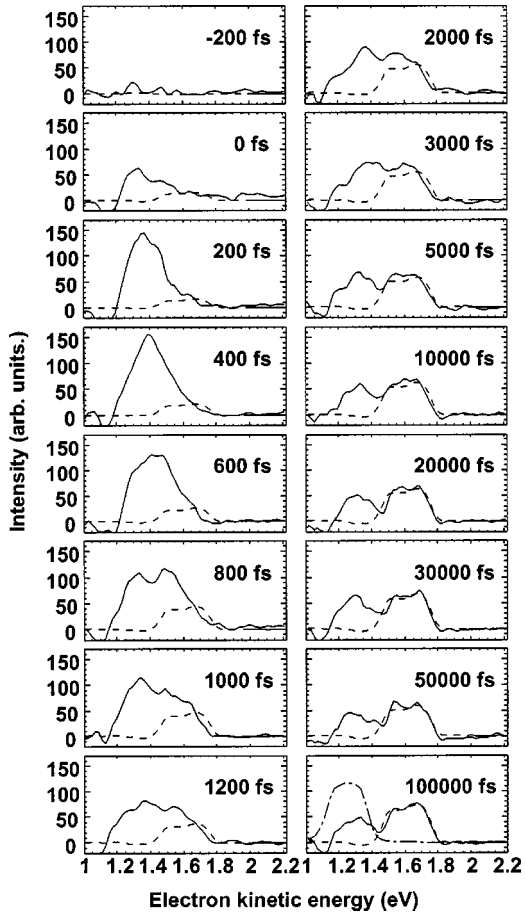

FIG. 4. Sequence of photoelectron spectra for pump–probe delay times between −200 fs and 100 ps using 395 nm pump pulses. The fitted contribution of I^- to each PE spectrum is shown as a dashed line. The remainder is assigned to excited $I^- \cdot CH_3I$ complexes (see text). The PE spectrum of cold $I^- CH_3I$ is shown as the dashed–dotted line in the last panel.

peak, but ~5 ps after the pump pulse a minimum starts to develop at 1.45 eV. This minimum becomes more pronounced for longer delay times, and the spectrum separates into two peaks centered at 1.3 and 1.6 eV. These two peaks show opposite temporal behavior: while the intensity of the peak at 1.3 eV decreases with time, the peak at 1.6 eV increases between 5 and 100 ps. This direct inspection of the measured spectra already shows that significant dynamics are occurring long after the pump pulse.

To complement these experimental results, we have calculated the structure of the precursor cluster $I_2^- \cdot CH_3I$ using GAUSSIAN 98 (Ref. 46) at the B3LYP/LANL2DZdp level of theory.[47] The calculation showed that the complex is essentially a slightly perturbed I_2^- molecule bound to CH_3I in an approximately T-shaped structure (see Fig. 1). The distance of the I_2^- dimer from the central carbon in $I_2^- \cdot CH_3I$ is calculated to be about 4 Å. This value is larger than the $I^- - C$ distance in the entrance channel complex of reaction (1), $I^- CH_3I$, which was calculated to be 3.4 Å.[34] The calculated angle between the I_2^- bond and symmetry axis of CH_3I is 80°.

IV. ANALYSIS

The dominant features in the pump–probe PE spectra can be assigned by comparison to probe-only PE spectra measured for the same experimental conditions. At $\lambda_{pump} = 790$ nm, the peak at 1.3 eV that emerges after 600 fs delay time (Fig. 3) looks very similar to the probe-only PE spectrum measured for $I^- \cdot CH_3I$ complexes produced in the ion source (upper panel in Fig. 2 and dashed–dotted line in Fig. 3). We thus assign the peak in the long-time pump–probe spectrum to the $I^- \cdot CH_3I$ fragment produced by photoexcitation of $I_2^- \cdot CH_3I$. The probe-only PE spectrum of $I^- \cdot CH_3I$ peaks at 1.25 eV. This 50 meV shift, compared to the long-time pump–probe PE spectra, is attributed to differences in ion temperature, because the $I^- \cdot CH_3I$ produced in the ion source should be vibrationally colder than the $I^- \cdot CH_3I$ photofragment. The weak tail that extends to higher photoelectron energies (1.5–1.8 eV) in the pump–probe PE spectra suggests that a small amount of bare I^- is also formed during the first 500 fs.

The peak at 1.3 eV in the pump–probe spectra is close in energy to the highest eKE peak in the probe-only PE spectrum of $I_2^- \cdot CH_3I$ (1.2 eV, Fig. 2), raising the possibility that the parent ion is reformed at least transiently by recombination of the I and I^- fragments. However, no signal was seen at 0.6 eV, the next highest eKE peak in the $I_2^- \cdot CH_3I$ spectrum, at any delay time, so the parent ion can be ruled out as the source of any signal in the pump–probe spectra.

At $\lambda_{pump} = 395$ nm, the two broad peaks that are seen for delay times >5 ps (Fig. 4) can also be assigned by comparison to probe-only spectra. The peak at 1.6 eV matches the PE spectrum of I^- to the $^2P_{3/2}$ state of neutral iodine (dashed line), and is assigned to bare I^- ejected from the $I^- \cdot CH_3I$ complex. The other spectral feature at 1.3 eV is assigned to vibrationally excited $I^- \cdot CH_3I$, just as for $\lambda_{pump} = 395$ nm. However, in contrast to the data for $\lambda_{pump} = 790$ nm, the single feature at delay times from 200 to 600 fs peaks at 1.4 eV; a peak at 1.3 eV is seen only after much longer delay times of about 5 ps. These observations suggest that excitation at 395 nm produces energized $I^- \cdot CH_3I$ (the peak at 1.4 eV) that decays to bare I^-, and that the vibrational energy distribution in the remaining $I^- \cdot CH_3I$ evolves on a time scale comparable to that over which dissociation occurs.

To investigate the dynamics induced by the 395 nm pump pulse more quantitatively, the intensities from photodetachment of I^- and $I^- CH_3I$ in Fig. 4 are derived for all pump–probe delay times. The intensity of the I^- peak is obtained by fitting its peak shape to the time-dependent spectra in the energy range between 1.65 and 1.8 eV, assuming that this high energy edge is solely due to an I^- feature, even for short pump–probe delay times. In Fig. 4, the fitted contributions of the I^- peak to the spectra are plotted as dashed lines. The $I^- \cdot CH_3I$ intensity is not derived in the same way, because the shape of this feature depends on its vibrational energy distribution which, we believe, varies with time. Instead, the $I^- CH_3I$ intensity is calculated as the difference between the intensity integral of the full spectrum and the intensity of the I^- peak.

In Fig. 5, the time-dependence of the derived $I^- \cdot CH_3I$ (▼) and I^- (▲) intensities is shown. These results are fit to the following biexponential curves,

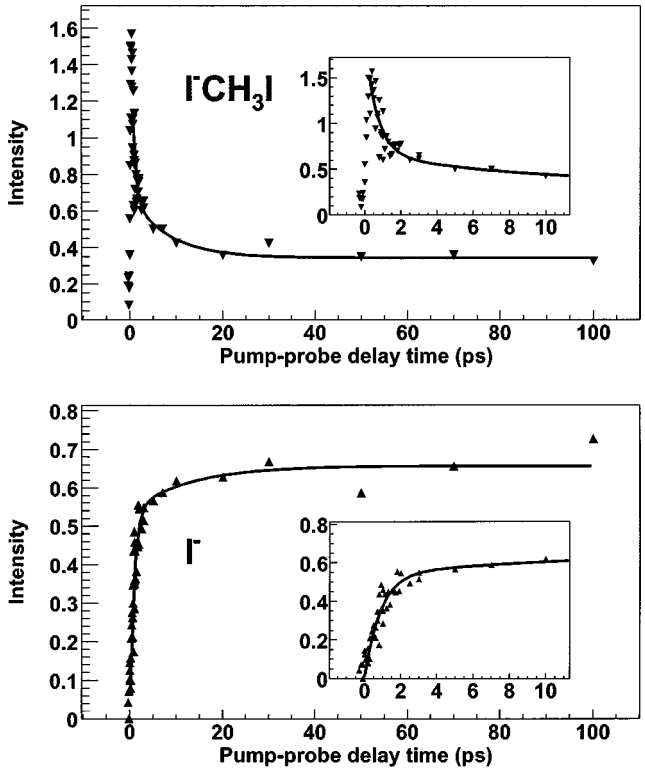

FIG. 5. Integral intensity of the contributions from $I^- \cdot CH_3I$ (upper panel) and I^- (lower panel) to the FPE spectra at $\lambda_{pump}=395$ nm. The I^- intensity is obtained from a fit to the photoelectron spectra (Fig. 4), whereas the $I^- \cdot CH_3I$ intensity is the difference of the total peak integrals in Fig. 4 and the fitted I^- intensity. Biexponential decay or growth curves, shown as solid lines, reproduce both intensity profiles [see Eq. (2) in text for fit functions and parameters].

$$
\begin{aligned}
I(t)_{I^-CH_3I} &= 1.6(0.78 \cdot \exp(-t/0.68\ \text{ps}) \\
&\quad + (1-0.78) \cdot \exp(-t/8.5\ \text{ps})) + 0.34, \\
I(t)_{I^-} &= 0.66(1 - 0.81 \cdot \exp(-t/0.87\ \text{ps}) \\
&\quad - (1-0.81) \cdot \exp(-t/12\ \text{ps})).
\end{aligned} \tag{2}
$$

These fits are shown as solid lines in Fig. 5. The $I^- \cdot CH_3I$ intensity (upper panel) is found to increase rapidly directly after the pump pulse, with a time constant indistinguishable from the laser cross correlation. It then decays biexponentially with time constants of 0.68 ps (see inset) and 8.5 ps. The I^-CH_3I intensity is fitted only from 200 fs onward, to exclude the fast initial rise. The I^- peak intensity (lower panel) exhibits first a fast increase, with a time constant of 0.87 ps, followed again by a slower increase with time constant 12 ps. The statistical accuracy of the time constants is estimated to be about 10%. Thus, according to the fit, about 80% of the time-dependent signal follows a fast exponential of about 0.75 ps, for both $I^- \cdot CH_3I$ and I^-. The remaining 20% of the signal undergoes a slower decrease or increase, respectively, with a time constant of about 10 ps. Within experimental accuracy, both curves reach constant intensities after 50 ps. Both intensities are normalized in such a way that the total intensity yields 1.0 in the 50–100 ps delay time interval, yielding limiting values as $t \rightarrow \infty$ of about 0.34 for I^-CH_3I and 0.66 of I^-.

V. DISCUSSION

The FPE spectra of $I_2^- \cdot CH_3I$ show rather different dynamics at the two pump wavelengths. At 790 nm, the dominant process is production of vibrationally excited $I^- \cdot CH_3I$, the time scale for which is on the order of 600 fs. More complicated dynamics occur at 395 nm. The signal attributed to $I^- \cdot CH_3I$ is seen immediately after dissociation. Much of this product exhibits biexponential decay to $I^- + CH_3I$ according to Eq. (2), but longer-lived products are also observed, as evidenced by the plateau in the $I^- \cdot CH_3I$ signal as shown in Fig. 5 at the longest times examined in our experiment (100 ps).

In order to understand the dissociation dynamics, we first assume the overall dynamics can be broken down into two steps, with the CH_3I acting as a spectator during dissociation of the I_2^-, and then the neutral I fragment acting as a spectator during subsequent interaction of the I^- with the CH_3I. At $\lambda_{pump}=790$ nm ($h\nu=1.57$ eV), I_2^- is excited to the $A'\,^2\Pi_{g,1/2}$ state which correlates to $I(^2P_{3/2})+I^-$. Since the bond dissociation energy of I_2^- is 1.01 eV,[48] the relative kinetic energy of the separated $I+I^-$ fragments is 0.56 eV. At $\lambda_{pump}=395$ nm (3.14 eV), dissociation occurs on the $B\,^2\Sigma_g^+$ state that correlates to $I^*(^2P_{1/2})+I^-$.[42] The spin–orbit splitting in iodine is 0.94 eV, so dissociation on this repulsive curve yields a relative kinetic energy of 1.19 eV. Although quenching of the I* from I_2^- photodissociation is observed to be quite efficient in larger clusters,[49] it is unlikely to be induced by a single CH_3I molecule.[50]

If dissociation of the chromophore is unaffected by the presence of the CH_3I, so that the fragments reach their asympotic velocities prior to any significant interaction with the CH_3I, the velocities of the I and I^- fragments will be equal and opposite, and the relative kinetic energy between the I^- fragment and CH_3I will then be 0.15 eV for $\lambda_{pump}=790$ nm and 0.32 eV at 395 nm. These values are expected to be upper bounds owing to the non-negligible interaction of CH_3I with I^- during the initial dissociation.[51] Nonetheless, they provide a useful starting point for understanding the differences between the dynamics at the two pump wavelengths. Specifically, if we assume that the attractive interaction between the I^- fragment and CH_3I is approximated by the solvent shift in the $I_2^- \cdot CH_3I$ PE spectrum, i.e., 0.30 eV, then at 790 nm, the I^- photofragment should not have sufficient kinetic energy to break free of the complex, whereas at 395 nm, at least some of the $I^- \cdot CH_3I$ should be formed with enough energy to dissociate, depending on the detailed collision dynamics. Our experimental results at the two pump wavelengths are in accord with these expectations.

The FPE spectra at 790 nm share features in common to those reported for $I_2^-(CO_2)_4$ at the same pump wavelength.[52] In both cases, there is a substantial change from 0 to 200 fs, the features seen at 200 fs shift toward lower eKE over the next several hundred fs, and no changes are observed at longer times. Drawing from this earlier work, we attribute the dynamics from 0 to 200 fs to dissociation of the I_2^- chromophore, and the shifting from 200 to 600 fs to interactions between the I^- fragment and the CH_3I. In the calculated geometry of the $I_2^- \cdot CH_3I$ complex, the I_2^- bond is nearly

perpendicular to the C–I bond in CH_3I (see Fig. 1), so the initial motion of the I^- fragment is away from the CH_3I. By 200 fs, treating the neutral I fragment as a spectator, what remains is an $I^- \cdot CH_3I$ complex with the C–I^- bond stretched well beyond its equilibrium value of 3.4 Å, but with insufficient energy to dissociate to $I^- + CH_3I$. In this configuration, the FPE spectrum represents that of I^- shifted by only a fraction of the solvent shift (380 meV) observed in vibrationally cold $I^- \cdot CH_3I$.[15] The evolution of the spectrum from 200 to 600 fs suggests that the energy released as this bond contracts from its outer turning point is partially dissipated in other vibrational modes of the complex, most of which are not Franck–Condon active, resulting in a smaller average C–I^- bond length and a shift in the FPE spectrum toward lower eKE. Based on classical trajectory studies by Hase and co-workers[35,37] on the analogous $Cl^- + CH_3Cl$ reaction, we would expect this dissipation of vibrational energy to involve the other ''soft'' intermolecular modes (i.e., the $I^- \cdots CH_3I$ stretch and bends) rather than the CH_3I internal modes.

Parson and co-workers[50] have shown that ''anomalous charge-switching'' can play a major role in the dynamics of photoexcited clusters of solvated I_2^-, where the solvent-induced asymmetry of the excess electronic charge in the ground state is reversed in the excited $A'\,^2\Pi_{g,1/2}$ and $B\,^2\Sigma_g^+$ states. As a result, the solvent molecules undergo considerable rearrangement in the excited states of the clusters, and this accounts for some of the dynamics observed experimentally in the FPE spectra of $I_2^-(CO_2)_n$ and $I_2^-(Ar)_n$ clusters.[52,53] These effects may well be present in $I_2^- \cdot CH_3I$ but should be relatively small because of its relatively symmetric, nearly T-shaped geometry.

At $\lambda_{pump} = 395$ nm, dissociation of the I_2^- chromophore results in production of energized $I^- \cdot CH_3I$ products, most of which dissociate within 20 ps of the pump pulse according to the biexponential kinetics given by Eq. (2). Dissociation of products is consistent with the energetic arguments presented at the beginning of this section, which indicated that the I^- photofragment is formed with slightly more energy (in the range of 20 meV or less) than that required for product dissociation. We should thus be able to compare our results to experimental and theoretical results on low energy $I^- + CH_3I$ collisions, keeping in mind the caveat that the initial conditions are more restricted in our experiment than in a ''full collision'' experiment. While no studies of the dynamics of this reaction have been reported, previous theoretical and experimental results for the symmetric $Cl^- + CH_3Cl$ reaction can be used to aid in the interpretation of our data.

The first issue to consider is whether the energized $I^- \cdot CH_3I$ complexes are dissociating to reactants or products. We obviously cannot tell from the PE spectra alone, since the reactants and products are indistinguishable. The calculated barrier height along the S_N2 reaction coordinate lies 70 meV above the $I^- + CH_3I$ reactants,[19] so it is unlikely that there is enough excess energy in the complexes to pass over this barrier. Even if there were, the measured reaction cross section for $Cl^- + CH_3Cl$ remains very small until the collision energy is significantly above the barrier height, because the barrier rises rather steeply for noncollinear Cl–C–Cl geometries.[6,11] Similar constraints should apply to $I^- + CH_3I$, particularly in our experiment where the initial $I_2^- \cdot CH_3I$ geometry disfavors collinear, near-zero impact parameter collisions between the I^- and CH_3I. Hence, it is reasonable to assume that no reaction is occurring in our experiment, and that instead we only observe dissociation back to reactants.

The biexponential time constants used to fit $I^- \cdot CH_3I$ decay and I^- production indicate the presence of ''fast'' and ''slow'' dissociation of the complex back to reactants. The fast time constant, 0.75 ps, is comparable to the vibrational period of the $I^- \cdots CH_3I$ symmetric stretching mode, for which the calculated harmonic frequency is 66 cm^{-1},[34] implying fairly direct dissociation dynamics in which the I^- undergoes a single, approximately elastic collision with the CH_3I before dissociating. The longer time constant, 10 ps, is indicative of multiple C$\cdots I^-$ collisions and suggests that there is some energy flow from the reaction coordinate into other vibrational and/or rotational modes of the complex. Note that the longer time constant is comparable to the 12 ps lifetime of the related $Cl^- \cdot CH_3Cl$ complex derived from an experimental measurement of the $Cl^- + CH_3Cl$ association rate.[9]

It is instructive to compare our results to classical trajectory calculations on the $Cl^- + CH_3Cl \rightarrow Cl^- \cdots CH_3Cl$ association reaction.[35,36] These calculations have explored the types of collisions that lead to complex formation, the flow of vibrational energy within the complex, and the lifetime of the complex with respect to dissociation back to reactants. The calculations have shown that complex formation is efficient over a fairly wide range of impact parameters (0–20 Å) and involves $T \rightarrow R$ energy transfer, in which orbital angular momentum is converted into rotational angular momentum of the complex. They also show that the CH_3Cl vibrational modes are inactive in the association reaction; vibrational energy flow occurs only among the $Cl^- \cdots CH_3Cl$ intermolecular modes. Finally, the calculations predict that the lifetime distribution of the complexes can be fit by a bi- or triexponential function,

$$N(t)/N(0) = \sum_i a_i \exp(-k_i t), \tag{3}$$

where $N(t)/N(0)$ is the fraction of complexes surviving at time t. The fitting parameters depend on the initial conditions, in particular the collision energy E_{rel} and rotational temperature T_{rot} of the CH_3Cl. As an example, for $E_{rel} = 0.5$ kcal/mol (20 meV) and $T_{rot} = 300$ K, the calculated lifetime distribution is fit using three rate constants: 1.1, 0.15, and 0.093 ps^{-1}, constants which are quite similar to those that fit our lifetime results using Eq. (2) above.

The similarities between our time-resolved experiments and the trajectory calculations, even though they involve two different systems, certainly suggest that the detailed dynamics seen in the calculations carry over to our experiments. For example, based on the calculated geometry of $I_2^- \cdot CH_3I$, the impact parameter describing the $I^- + CH_3I$ interaction should be on the order of several Å, i.e., within the range where complex formation should be efficient. In addition, the multiexponential fit to the calculated $Cl^- \cdots CH_3Cl$

lifetimes, Eq. (3), is attributed to nonrandom vibrational energy distribution in the complex at short delay times,[35,37] so-called ''apparent non-RRKM behavior,'' [54] in which the decay rate varies as the vibrational energy distribution of the complex evolves. We interpret the biexponential $I^- \cdot CH_3I$ decay dynamics in our experiment as arising from similar effects, in which case our time-resolved results provide additional experimental evidence for nonstatistical dynamics on the S_N2 potential energy surface. This interpretation is also consistent with the experimentally observed shifting of the $I^- \cdot CH_3I$ peak toward lower eKE (from 1.4 to 1.3 eV) after 600 fs alluded to in Sec. IV. The shifting most likely reflects vibrational energy flow from the initially stretched $C \cdots I^-$ bond into other vibrational modes, and one expects the decay rate to decrease as this process occurs because of decreased excitation in the reaction coordinate.

The origin of $I^- \cdot CH_3I$ signal that persists out to 100 ps in our experiments is also of interest. This signal may simply result from bound complexes with insufficient energy to dissociate; the relative $I^- + CH_3I$ kinetic energy calculated in our ''two-step'' mechanism is barely enough for dissociation to occur, and any lowering of the energy owing to three-body interactions in the I_2^- dissociation process can result in the production of $I^- \cdot CH_3I$ with insufficient energy to dissociate. Effects of this type have been seen in photoinitated reactions in van der Waals complexes.[51] On the other hand, the classical trajectory calculations on $Cl^- + CH_3Cl$ at low collision energies show that some complexes do not dissociate for at least 20 ps, the maximum collision time in the calculations, and we may be forming analogous long-lived species in our experiments. Such a result is of interest in light of recent quantum mechanical scattering calculations that have predicted the existence of long-lived resonance states on the $Cl^- + CH_3Cl$ surface.[55,56]

VI. CONCLUSION

We have investigated the reaction dynamics of the symmetric S_N2 reaction of I^- with CH_3I in real time by femtosecond pump–probe photoelectron spectroscopy of the precursor complex $I_2^- \cdot CH_3I$. By photodissociating the I_2^- chromophore with a pump pulse, the neutral iodine fragment was driven away from the S_N2-reactants I^- and CH_3I, allowing us to follow their subsequent dynamics. Immediately after the pump pulse the reactants form an $I^- \cdot CH_3I$ complex, with an internal energy dependent on the energy of the pump photon. For 790 nm pump photons only stable complexes are observed, while with 395 nm pump photons about two thirds of the complexes decayed back to the reactants, $I^- + CH_3I$, on the time scale of the experiment (<100 ps). These unstable complexes exhibit bi-exponential dissociation dynamics: 80% decay with a fast time constant of about 0.75 ps and 20% with a slow time constant of about 10 ps. This biexponential decay and the observed shift of the $I^- CH_3I$ photoelectron peak during a time span of about 5 ps are indicative of ''apparent non-RRKM behavior'' of the complex, reflecting the evolution of vibrational energy flow in the complex on a time scale comparable to or slower than dissociation. The observed dynamics are similar to those seen in classical trajectory calculations on entrance channel complexes formed in bimolecular $Cl^- + CH_3Cl$ collisions.

This experiment represents an extension of the field of time-resolved bimolecular reaction studies to ion–molecule reactions and in particular to the fundamentally interesting class of S_N2-reactions. It is expected that further time-resolved studies on S_N2 reactions will shed more light on their dynamics, in particular on the coupling of the different inter- and intramolecular vibrations in the course of the reaction. In the future, studies of nonsymmetric S_N2-reactions are planned, a goal that will be aided by improved cluster ion preparation techniques.

ACKNOWLEDGMENTS

This research is supported by the National Science Foundation under Grant No. CHE-0092574. R.W. acknowledges support from the Alexander von Humboldt-Stiftung and from the Emmy Noether-Programm of the Deutsche Forschungsgemeinschaft.

[1] W. L. Hase, Science **266**, 998 (1994).
[2] M. L. Chabinyc, S. L. Craig, C. K. Regan, and J. I. Brauman, Science **279**, 1882 (1998).
[3] W. L. Hase, H. Wang, and G. H. Peslherbe, Adv. Gas Phase Ion Chem. **3**, 125 (1998).
[4] J. K. Laehdahl and E. Uggeruk, Int. J. Mass. Spectrom. **214**, 277 (2002).
[5] W. N. Olmstead and J. I. Brauman, J. Am. Chem. Soc. **99**, 4219 (1977).
[6] S. E. Barlow, J. M. V. Doren, and V. M. Bierbaum, J. Am. Chem. Soc. **110**, 7240 (1988).
[7] C. H. DePuy, S. Gronert, A. Mullin, and V. M. Bierbaum, J. Am. Chem. Soc. **112**, 8650 (1990).
[8] K. Giles and E. P. Grimsrud, J. Phys. Chem. **97**, 1318 (1993).
[9] C. Li, P. Ross, J. E. Szulejko, and T. B. McMahon, J. Am. Chem. Soc. **118**, 9360 (1996).
[10] S. L. Craig and J. I. Brauman, J. Am. Chem. Soc. **118**, 6786 (1996).
[11] V. F. DeTuri, P. A. Hintz, and K. M. Ervin, J. Phys. Chem. A **101**, 5969 (1997).
[12] S. Kato, G. E. Davico, H. S. Lee, C. H. DePuy, and V. M. Bierbaum, Int. J. Mass. Spectrom. **210/211**, 223 (2001).
[13] C. K. Regan, S. L. Craig, and J. I. Brauman, Science **295**, 2245 (2002).
[14] S. T. Graul, C. J. Carpenter, J. E. Bushnell, P. A. M. v. Koppen, and M. T. Bowers, J. Am. Chem. Soc. **120**, 6785 (1998).
[15] D. M. Cyr, G. A. Bishea, M. G. Scarton, and M. A. Johnson, J. Chem. Phys. **97**, 5911 (1992).
[16] C. E. H. Dessent, C. G. Bailey, and M. A. Johnson, J. Chem. Phys. **105**, 10416 (1996).
[17] P. Ayotte, J. Kim, J. A. Kelley, S. B. Nielsen, and M. A. Johnson, J. Am. Chem. Soc. **121**, 6950 (1999).
[18] H. Wang, L. Zhu, and W. L. Hase, J. Phys. Chem. **98**, 1608 (1994).
[19] M. N. Glukhovtsev, A. Pross, and L. Radom, J. Am. Chem. Soc. **117**, 2024 (1995).
[20] S. Schmatz, Chem. Phys. Lett. **330**, 188 (2000).
[21] T. I. Solling, A. Pross, and L. Radom, Int. J. Mass. Spectrom. **210/211**, 1 (2001).
[22] S. Raugei, G. Cardini, and V. Schettino, J. Chem. Phys. **114**, 4089 (2001).
[23] S. Schmatz, P. Botschwina, J. Hauschildt, and R. Schinke, J. Chem. Phys. **114**, 5233 (2001).
[24] A. A. Viggiano, R. A. Morris, J. S. Paschkewitz, and J. F. Paulson, J. Am. Chem. Soc. **114**, 10477 (1992).
[25] L. Sun, K. Song, and W. L. Hase, Science **296**, 875 (2002).
[26] D. C. Clary, Science **279**, 1879 (1998).
[27] D. M. Neumark, Annu. Rev. Phys. Chem. **52**, 255 (2001).
[28] M. T. Zanni, V. S. Batista, B. J. Greenblatt, W. H. Miller, and D. M. Neumark, J. Chem. Phys. **110**, 3748 (1999).
[29] B. J. Greenblatt, M. T. Zanni, and D. M. Neumark, Science **276**, 1675 (1997).
[30] A. V. Davis, R. Wester, A. E. Bragg, and D. M. Neumark, J. Chem. Phys. **117**, 4282 (2002).

[31] D. M. Cyr, C. G. Bailey, D. Serxner, M. G. Scarton, and M. A. Johnson, J. Chem. Phys. **101**, 10507 (1994).
[32] D. M. Cyr, M. G. Scarton, and M. A. Johnson, J. Chem. Phys. **99**, 4869 (1993).
[33] C. C. Arnold, D. M. Neumark, D. M. Cyr, and M. A. Johnson, J. Am. Chem. Soc. **99**, 1633 (1995).
[34] W. Hu and D. G. Truhlar, J. Phys. Chem. **98**, 1049 (1994).
[35] S. R. Vande Linde and W. L. Hase, J. Chem. Phys. **93**, 7962 (1990).
[36] W. L. Hase and Y. J. Cho, J. Chem. Phys. **98**, 8626 (1993).
[37] G. H. Peslherbe, H. Wang, and W. L. Hase, J. Chem. Phys. **102**, 5626 (1994).
[38] C. Jouvet and B. Soep, Chem. Phys. Lett. **96**, 426 (1983).
[39] S. Buelow, G. Radhakrishnan, J. Catanzarite, and C. Wittig, J. Chem. Phys. **83**, 444 (1985).
[40] H. Ohoyama, M. Takayanagi, T. Nishiya, and I. Hanazaki, Chem. Phys. Lett. **162**, 1 (1989).
[41] N. F. Scherer, C. Sipes, R. B. Bernstein, and A. H. Zewail, J. Chem. Phys. **92**, 5239 (1990).
[42] P. E. Maslen, J. Faeder, and R. Parson, Chem. Phys. Lett. **263**, 63 (1996).
[43] B. J. Greenblatt, M. T. Zanni, and D. M. Neumark, Faraday Discuss. **108**, 101 (1998).
[44] H. Hotop and W. C. Lineberger, J. Phys. Chem. Ref. Data **14**, 731 (1985).
[45] K. R. Asmis, T. R. Taylor, C. Xu, and D. M. Neumark, J. Chem. Phys. **109**, 4389 (1998).
[46] M. J. Frisch *et al.*, GAUSSIAN 98, Revision A.9, Gaussian, Inc., Pittsburgh PA, 1998.
[47] C. E. Check, T. O. Faust, J. M. Bailey, B. J. Wright, T. M. Gilbert, and L. S. Sunderlin, J. Phys. Chem. A **105**, 8111 (2001).
[48] M. T. Zanni, T. R. Taylor, B. J. Greenblatt, B. Soep, and D. M. Neumark, J. Chem. Phys. **107**, 7613 (1997).
[49] A. Sanov, S. Nandi, and W. C. Lineberger, J. Chem. Phys. **108**, 5155 (1998).
[50] R. Parson, J. Faeder, and N. Delaney, J. Phys. Chem. A **104**, 9653 (2000).
[51] G. Hoffmann, D. Oh, Y. Chen, Y. M. Engel, and C. Wittig, Isr. J. Chem. **30**, 115 (1990).
[52] B. J. Greenblatt, M. T. Zanni, and D. M. Neumark, J. Chem. Phys. **112**, 601 (2000).
[53] B. J. Greenblatt, M. T. Zanni, and D. M. Neumark, J. Chem. Phys. **111**, 10566 (1999).
[54] D. L. Bunker and W. L. Hase, J. Chem. Phys. **59**, 4621 (1973).
[55] D. C. Clary and J. Palma, J. Chem. Phys. **106**, 575 (1997).
[56] S. Schmatz and J. Hauschildt, J. Chem. Phys. **118**, 4499 (2003).